RNA Stores Tau Reversibly in Complex Coacervates

Xuemei Zhang[1,4], Neil A. Eschmann[2], Yanxian Lin[3], Hongjun Zhou[1,4], Jennifer Rauch[1,4], Israel Hernandez[1,4], Elmer Guzman[1,4], Kenneth S. Kosik[*,1,4], Songi Han[*,2,3,5]

[1] Molecular, Cell and Developmental Biology, University of California Santa Barbara, Santa Barbara, CA 93106, USA.

[2] Department of Chemistry and Biochemistry, University of California Santa Barbara, Santa Barbara, CA 93106, USA.

[3] Biomolecular Science and Engineering, University of California Santa Barbara, Santa Barbara, CA 93106, USA.

[4] Neuroscience Institute, University of California Santa Barbara, Santa Barbara, CA 93106, USA.

[5] Department of Chemical Engineering, University of California Santa Barbara, Santa Barbara, CA 93106, USA.

*Correspondence to: kenneth.kosik@lifesci.ucsb.edu; songi@chem.ucsb.edu

Competing interests

The authors declare no competing financial interests.

Contributions

K.S.K. and S.H. designed experiments; X.Z. did the PAR-iCLIP experiments, the *in vitro* RNA-protein binding assays; E.G. sequenced the DNA libraries; H.Z. performed bioinformatics

analysis; J.R. did ITC experiments; N.A.E., Y.L. and J.R. did the RNA-Tau *in vitro* droplet formation; N.A.E. did EPR and DEER experiments; I.H. did sarkosyl fractionation; Y.L. and H.Z., contributed to manuscript preparation; X.Z., K.S.K. and S.H. wrote the manuscript.

Abstract

Non-membrane bound organelles that behave like liquid droplets are widespread among eukaryotic cells. Their dysregulation appears to be a critical step in several neurodegenerative conditions. Here we report that Tau protein, the primary constituent of Alzheimer neurofibrillary tangles, can form liquid droplets and therefore has the necessary biophysical properties to undergo a liquid-liquid phase separation (LLPS) in cells. Consonant with the factors that induce LLPS, Tau is an intrinsically disordered protein that electrostatically complexes with RNA to form droplets that can be tuned by salt concentration and temperature and exhibit low interfacial tension. Uniquely, the pool of RNAs to which Tau binds in living cells are tRNAs. This phase state of Tau is held in 1:1 charge balance across large blocks of the protein and the nucleic acid and forms optimal complexes at multiple RNA:Tau mass ratios. These features define a complex co-acervate in which undergo free diffusion in their interior, despite the high concentration of protein, and rapid exchange with their exterior environment. Counter to most closely packed protein assemblies, the condensed phase state of Tau is not associated with changes in local Tau conformations as verified by distance measurements across a pair of spin labels by pulsed dipolar spectroscopy. In contrast, fibrillar states of Tau are accompanied by large changes in local Tau conformations. Importantly, prolonged residency within a droplet results in the emergence of detectable beta-structure by thioflavin labeling, suggesting that the droplet state can incubate Tau and pre-dispose it toward beta sheet structures typical of insoluble Tau fibrils.

Introduction

Inclusions consisting of the Tau protein occur in many neurological conditions with Alzheimer's disease the most prominent among them. Normally, Tau is in a kinetic equilibrium between a microtubule bound and free state. Under disease conditions Tau self-assembles into fibrils that eventually lead to highly insoluble polymeric inclusions known as neurofibrillary tangles. The underlying biophysical basis for the transition of Tau from a microtubule-associated protein to an insoluble fibril is unknown. However, a clue comes from the observation that polyanions, such as heparin, promote Tau fibrillization [1]. Although less effectively, RNA can also induce Tau fibrillization [2, 3], and unlike heparin, RNA is present intracellularly, making it accessible to interact with Tau.

Our experiments began with the finding that Tau can bind RNA in living cells and interestingly Tau-RNA binding shows selectivity for tRNAs. This observation along with the known categorization of Tau as intrinsically disordered and its ability to spread from cell to cell in a manner that resembles prions [4, 5], suggested that Tau might share additional properties with other RNA binding proteins involved in neurodegeneration. These proteins include FUS [6], TDP-43 [7], C9ORF72 [8, 9], hnRNPA2B1 and hnRNPA1 [10, 11] all of which can undergo liquid-liquid phase-separation from the surrounding aqueous medium into droplets *in vitro*. These highly protein dense structures, known in the chemical literature as complex coacervates [12, 13], establish a liquid liquid phase state (LLPS) associated with (1) increasing protein concentration, (2) tuning the salt concentration and temperature, (3) the presence of RNA complexed to an intrinsically disordered protein and (4) low interfacial tension to promote fusion. A consensus property of a complex coacervate is high internal fluid dynamics rooted in low

cohesive energy between the polyelectrolyte complexes and weakly bound water constituting the fluid [13, 14]. Complex coacervate chemistry has facilitated bio-inspired coating, wet adhesion and engulfment [15-17].

Here we show that Tau-RNA complexes have all the properties of a complex coacervate. When multiple Tau molecules weakly bind RNA and overall charge matching is achieved between the polycation, Tau, and polyanion, RNA, Tau undergoes condensation and phase separation into micrometer sized droplets. Remarkably, within this liquid phase-separated state Tau maintains internal segment mobility and a compact conformation between two spin labels around the core region of Tau known as PHF6(*) despite the molecular crowding associated with coacervation. In contrast, this region undergoes irreversible fibrillization in the presence of a different polyanion, heparin, which induces full extension of Tau monomers and packs monomers into β-sheet assemblies. The spontaneous and reversible droplet formation suggests that Tau is held in a low energy-barrier fluid state between dilute solution and complex coacervate condensate with the free energy difference toggled by interactions mediated by ions. However, prolonged residence in this phase state begins to induce β-sheet formation suggesting that the highly condensed phase state of Tau is a precursor to fibril formation.

Results

Tau binds RNA in living cells

RNA binding to Tau in living cells was examined by PAR-iCLIP using the human Tau-specific antibody, HJ 8.5, in HEK 293T cells, human iPSC-derived neurons and retinoic acid-differentiated neuroblastoma SH-SY5Y cells. The HEK 293T cells expressed wild type full-length human Tau (4R2N), mutant Tau (P301L-4R2N) or mutant Tau fused to CFP (P301L,

4R1N) (Fig. 1a-b, Fig. S1, Fig. S2a-c). iPSC-derived neurons were derived from carriers of 4R2N Tau (Fig. 1c), P301L Tau or a risk variant for progressive supranuclear palsy, A152T. The SH-SY5Y cells expressed both Tau and the short isoform of MAP2 called MAP2c [18] (Fig. S2d). Strong binding of Tau to RNA was observed in all cells, as indicated by ^{32}P-labeled RNA bands corresponding to immunoprecipitated and cross-linked Tau-RNA complexes (Fig. 1a-c, lanes 2; Fig. S2a, lane 2). The radioactive Tau-bound RNA band was found to run as 30-100 nt (data not shown). PAR-iCLIP experiments with varying RNase concentrations did not shift the ^{32}P-labeled band, nor change its intensity (lanes 2-3 in Fig. S2b). These experiments indicate that in contrast to most known RNA-binding proteins that bind to RNA as a smear over a range of sizes, Tau binds specifically and dominantly to small RNAs or RNA fragments.

Because small RNAs are abundant and may engage in non-specific interactions, we performed multiple confirmatory controls (Fig. S2b lanes 1, 4 and S2c lanes 3, 4), including immunoprecipitation in HEK cells without Tau expression, without Tau antibody to rule out non-specific binding and without UV exposure to eliminate the possibility that Tau-RNA complexes formed *in vitro* after cell lysis. Various disease mutations of Tau had no effect on the binding to RNA in either the HEK cells or the human iPSC-derived neurons. Although Tau and MAP2 are highly homologous in their proline rich and microtubule binding domains, MAP2 did not bind RNA (Fig. S2d, lane 3).

To identify the RNA types crosslinked to Tau, DNA libraries were prepared from the immunoprecipitated radiolabeled bands and sequenced. In all experiments, the controls consistently showed relatively few total reads and very few uniquely aligned reads (Fig. S2e-f). We analyzed the distribution of Tau-bound RNA from the human genome by defining eight regions: exons, introns, lincRNAs, snRNAs, rRNAs, miRNAs, tRNAs and intergenics. In Tau-

113 expressing HEK cells, tRNAs were overwhelmingly the highest category of RNA crosslinked to
114 Tau (Fig. 1d). Endogenous Tau in hiPSC-derived neurons also bound tRNAs; however,
115 background RNA from introns and intergenics were relatively abundant as well (Fig. 1e).
116 Background RNA sequences are common in all CLIP studies, particularly for atypical RNA
117 binding proteins [19]. Despite the abundance of tRNAs in cells however, background reads from
118 CLIP experiments consistently show a paucity of tRNAs. Correcting for background reads by
119 dividing the percentage of Tau-bound RNA by the percentage of nucleotides of each category in
120 the genome demonstrated a selective enrichment of tRNAs (Fig. 1f-g). The specific tRNA
121 species crosslinked to Tau overlapped extensively between HEK and hiPSC-derived neuron
122 samples. Of 625 annotated tRNA loci in the human genome, 462 tRNA genes crosslinked to Tau
123 in HEK cells with 79% of them observed in all four Tau CLIP samples and 94% in at least two
124 samples. In the hiPSC-derived neurons, all 231 tRNA genes identified were also observed in the
125 HEK cells and 119 of these were verified in at least two Tau CLIP samples. The distribution of
126 the cross-linked tRNAs in HEK and hiPSC-derived neurons differed from the distribution of the
127 total tRNAs. This difference indicated that the tRNAs selected by the CLIP experiment were not
128 randomly drawn from the total tRNA pool (Fig. S3a-b). Among the most differentially selected
129 tRNAs by CLIP was $tRNA^{Arg}$ (Fig. S3c).

130 PAR-iCLIP can identify the cross-linked sites in the tRNAs. tRNA sequences extend
131 from the most 3' nucleotide of the tRNA to the covalently cross-linked site where the sequencing
132 terminates. In both HEK cells and hiPSC-derived neurons, the crosslink site was predominantly
133 located within the anti-codon loop (Fig. 2a-b, Fig. S4), followed by the T loop and in the D-loop,
134 both with far smaller frequencies. Overall there was a preference for single-strand segments of
135 tRNA as crosslink sites.

136

137 **Tau-RNA Binding Affinity and Stoichiometry**

138 A gel shift assay using recombinant wild type full-length human Tau (4R2N) induced a
139 shift in unacetylated $tRNA^{Lys}$ (Fig. 3a), yielding a dissociation constant (K_d) for 4R2N Tau
140 binding to tRNA of 460 ± 47 nM (Fig. 3b). The derived Hill coefficient was 2.8, implying
141 cooperative binding of multiple Tau proteins to tRNA [20]. Isothermal titration calorimetry (ITC)
142 experiments independently confirmed the affinity of Tau binding to tRNA to yield K_d = 735 ±
143 217 nM and 372 ± 9 nM for 4R2N and K18 Tau, respectively (Fig. 3c). The dissociation constant
144 for 4R2N Tau binding to a 43 nucleotide random RNA sequence still yielded a K_d = 832 ± 94 nM
145 with a Hill coefficient of 2.6 according to a gel shift assay, suggesting that Tau effectively binds
146 RNA non-specifically *in vitro*, although there may be differences in binding affinity.

147 Our *in vitro* observation further suggested that Tau binds RNA in two stages, first
148 forming a protein dimer-RNA (P_2R) complex followed by a protein multimer-RNA ($P_{2n}R$)
149 complex, consistent with a two-stage RNA binding model reported for the protein AUF1 [21]
150 and hnRNP A1 [22]. The ITC titration experiments showed that both 4R2N and K18 Tau interact
151 with tRNA with the stoichiometry of a protein dimer (Fig. 3c, n = 0.52 ± 0.04), while the gel
152 shift assay showed multiple bands corresponding to high molecular weight protein-RNA
153 complexes. These include a faster migrating band representing P_2R complexes populated at
154 lower Tau:tRNA molar ratio and a slower migrating band representing $P_{2n}R$ complexes
155 populated at higher Tau:tRNA molar ratios (Fig. 3d-e). The fraction of bound Tau (from the low
156 or high bands) was plotted as a function of Tau:tRNA molar ratios (Fig. 3f), and compared to the
157 theoretical binding saturation curves for 1:1 to 6:1 binding stoichiometries (Fig. 3f). At lower
158 Tau:tRNA molar ratios, Tau and RNA form complexes at a ~2:1 ratio, while at higher Tau:tRNA

159 molar ratios, Tau and tRNA form complexes at ratios up to 6:1. We conclude that tRNA is
160 capable of binding multiple Tau proteins in a multi-step process. Judging by the absence of
161 higher stoichiometric signatures in the ITC measurement that is less sensitive to binding events
162 associated with small changes in heat, Tau:tRNA complexes that exceed a ratio of 2:1 must rely
163 on weak interactions.
164
165 **Tau phase-separates in the presence of RNA**
166 Mixing of 4R2N or Δtau187 (similar to K18, see Methods section) constructs with tRNA
167 (25 kDa), poly(A) RNA (66~660 kDa) or poly(U) RNA (800~1000 kDa) reliably produced a
168 turbid solution under a wide range of Tau:RNA mass ratios and salt concentrations (Fig. 4a-e and
169 Fig. S5a-e). According to bright-field microscopy (Fig. 4a), droplets formed and phase separated
170 from the bulk aqueous phase with a clearly visible and highly spherical boundary. Tau droplets
171 were capable of merging into a single droplet with the complete and nearly instantaneous loss of
172 any boundary at the fusion interface, indicating that the droplets are fluidic with a relatively low
173 interfacial tension (a series of snapshots capturing the fusion of two droplets are shown in Fig.
174 4a). Confocal microscopy images of fluorescence-labeled Tau verify that Tau is exclusively and
175 homogenously contained within the droplet (Fig. 4b).
176
177 **Tau-RNA droplets form a complex coacervate phase**
178 Droplet formation follows from the mixing of two oppositely charged biopolymers at a given
179 pH—Tau and RNA. Systematic increase in the salt concentration decreased the number of Tau-
180 RNA droplets that eventually disappeared when the salt concentration was increased to 100 mM
181 or higher (Fig. 4c-d, Fig. S5a left panel). Droplet formation was maximal at Δtau187:tRNA

molar ratios of 8:1, Δtau187:poly(A) RNA molar ratios from 33:1 to 330:1 and Δtau187:poly(U) RNA ratios from 267:1 to 333:1 (estimated from the molecular weight of RNAs, see Fig. S5c). Remarkably, each of these stoichiometries converge to a Δtau187:tRNA charge ratio of ~1:1, irrespective of the RNA type (Fig. 4e, Fig. S5a right panel). Droplet formation was also observed with full length Tau 4R2N and RNA, but was less robust than with Δtau187, possibly due to the additional negative charges at the N-terminal segment of Tau 4R2N that would diminish the electrostatic association between Tau and RNA. However, at pH 6 where the net charge of Tau 4R2N is similar to Δtau187, droplets reliably formed, though yielding lower number densities, and were exquisitely sensitive to salt concentration (Fig. S5e). Even at NaCl concentrations as low as 10 mM, the droplets dissolved. In cellular environments however, additional factors—charged co-constituents or posttranslational modifications of Tau—may strengthen Tau-RNA associations, rendering droplet formation more favorable at higher ionic strengths. Together, these observations show that droplet formation is dominated by electrostatic complexation between oppositely charged polyelectrolytes, while the shielding of their excess charge (by the tuning of Tau:RNA ratio) is critical to form an extended assembly constituting the droplets. From this we conclude that Tau-RNA droplet formation follows a complex coacervation mechanism, initiated through non-specific complexation of oppositely charged polyelectrolytes and driven by the further association of these polyelectrolyte complexes to form a macroscopic fluid phase by relying on weak electrostatic attractions tuned by salt concentration [23]. A crucial observation is that complex coacervate droplet formation is spontaneous and fully reversible through the tuning of salt concentration and Tau:RNA ratios. The convergence of different Tau constructs toward the shared property of complex coacervation with different RNA

species present at a common charge ratio of ~1:1 leads us conclude that complex coacervate-driven droplet formation is an intrinsic property of Tau in the presence of RNA.

Tau in condensed droplets is in a solution state

Within a condensed complex coacervate, held together by non-specific and weak electrostatic interactions, we expect the polyelectrolyte constituents to maintain their hydration layer and remain dynamic [14, 24]. To spectroscopically track Tau exclusively from within the condensed phase we first positively verified by confocal fluorescence imaging that Δtau187 was exclusively localized within the droplet (Fig. 4b). This allowed us to characterize the droplet-internal protein properties. First, continuous wave electron paramagnetic resonance (cw EPR) spectral line shape analysis of singly spin labeled Δtau187 at cysteine site 322, Δtau187/322C-SL, diluted with diamagnetically labeled Δtau187/322C-DL (see Methods), was used to compare the protein side chain dynamics and degrees of freedom of the tethered spin label of Δtau187 in dilute solution state (Fig. 4 red, f-h), in the droplet state associated with poly(A) RNA (blue, f) and tRNA (green, g) and upon addition of the Tau aggregation inducer, heparin (black, h). Remarkably, the EPR lineshape of Δtau187/322C-SL within the droplet phase was indistinguishable from the dilute solution state (Fig. 4f vs. 4g). In contrast, the EPR line shape dramatically broadened within minutes of adding heparin—a highly effective aggregation inducer of Tau [1, 25] (Fig. 4f vs. 4h). This finding demonstrates that the condensation of Δtau187 to high protein concentration alone does not effectively induce dehydration and aggregation of Tau, and that Tau remains dynamic and hydrated and retains protein dynamical properties as found in solution state, despite forming long-range associations with RNA in a highly condensed fluid phase.

To determine whether Tau assumes altered protein conformations in the complex coacervate phase compared to the dilute solution phase, we compared the PHF6 and PHF6* hexapeptide regions of Tau under these conditions. These regions of the Tau sequence pack into the β-sheet core once fibrils are formed of Tau [26]. Previously, we identified that both the PHF6 and PHF6* hexapeptide regions of Tau undergo a dramatic opening from a compact to a fully extended local conformation within minutes of adding heparin, well before fibril formation is seen and remain extended as insoluble fibrils are formed (unpublished data). These local distance measurements of the regions flanking the PHF6(*) regions offer a powerful tool to compare the conformational state of Tau in dilute solution, droplet and aggregation-induced states. We prepared a Δtau187 G272C/S285C-SL_2 construct that was doubly MTSL-labeled at sites 272 and 285 (see Methods) to access the distances across the PHF6* hexapeptide region by double electron-electron resonance (DEER) spectroscopy. Surprisingly, the distances flanking the PHF6* region remained unchanged from dilute solution state to when Tau was condensed into a concentrated complex coacervate phase in association with poly(A) RNA and tRNA (Fig. 4i and j). This contrasts with the effect of heparin on Tau that markedly extended the segment distances (from ~3 to ~4 nm) between the labels, within minutes of heparin addition, corresponding to the extended conformation that the PHF6(*) segment adopts in insoluble fibrils when neatly stacked in β-sheets (Fig. 4k).

Interestingly, we observed a low-level Thioflavin T (ThT) signal under Tau-poly(U) RNA droplet forming conditions (see Fig. S5f) that gradually increased with time over 12 hours. This ThT signal was nearly entirely diminished at increased salt concentration at which Tau-RNA associations are weakened and droplets are resolved. Still, the ThT intensity from the Tau-RNA droplet samples, even after three days of incubation, was significantly smaller (less than

5%) compared to what was observed in the presence of the aggregation-inducing heparin under similar charge ratio and mass concentration at any incubation time (Fig. S5f). Since ThT intensity is commonly used as an assay to map β-sheet content, we suggest that droplet formation through association with RNA increases the aggregation propensity of Tau *in vitro*, even while the Tau-RNA complexes are held together by fully reversible weak interactions.

Exogenous tRNA can induce sarkosyl insolubility of Tau

To determine whether Tau-RNA complexes have the potential for pathological interactions *in vivo*, hiPSC-derived neurons with a P301L mutation or wild type were transfected with 20U tRNA per 1.2 million cells. Cell lysates (input) were prepared in a high salt/high sucrose buffer, followed by fractionation in a 1% sarkosyl buffer. Transfection in the absence of nucleic acids (mock) or addition of tRNA to the mock lysate (mock + tRNA) were used as controls. Cells transfected with tRNA accumulated sarkosyl insoluble Tau, whereas cells without added tRNA or when tRNA was added to the lysis buffer did not increase Tau in the insoluble fractions (Fig. 5). The increase in sarkosyl-insoluble Tau populations occurred in both wild-type and P301L Tau-containing cells when infected with tRNA.

Discussion

Tau can bind RNA in two stages, mediated by (i) strong binding at a Tau:RNA molar ratio of 2:1 with nanomolar dissociation constants and (ii) weak association between Tau multimers and RNA to form higher order complexes. Although Tau lacks a recognizable RNA-binding motif, it bound tRNA as its dominant partner *in vivo*. Furthermore, Tau was found to spontaneously phase separate upon non-specific complexation with RNA into dense protein

droplets, whose formation was reversibly and sensitively tunable by salt concentrations, as well as the Tau:RNA ratios. Crucially, the optimal Tau:RNA molar ratios range from 8:1 to 330:1, which varies among different RNA species. Remarkably, all higher order complexes converge to a common Tau:RNA charge ratio of ~1:1, leading us to conclude that Tau-RNA droplet formation is driven by electrostatic interactions underlying complex coacervation, in which oppositely charged polyelectrolytes associate into extended assemblies held together by weak electrostatic interactions and condense to a macroscopic fluid phase [14, 17, 27].

Crucially, Tau complexed with RNA in the highly condensed droplet state maintains the dynamical and conformational signature of free Tau in solution state according to cw EPR and DEER analysis around the β-sheet forming PHF6(*) segment of Tau, implying that small changes in the free energy of Tau accompany its condensation to the droplet phase. At the same time, a low-level ThT signal was observed from the Tau-RNA droplet samples after extensive incubation time, though significantly weaker compared to from Tau solutions *en route* to fibrils as initiated by the addition of heparin. Nevertheless, the implication that Tau droplets have some propensity toward soluble β-sheet complexes suggests that complexation with RNA under droplet forming conditions may be on pathway to fibrils. Consistent with this finding, tRNA increased sarkosyl insolubility of Tau *in vivo*. We conclude that dynamic and free Tau species are stored in the concentrated droplet state that, on the one hand is predisposed to convert to fibrils, and on the other hand can spontaneously and reversibly dissolve into solution at increased salt concentration. This previously unrecognized droplet phase state contrasts with that of Tau following incubation with the polyanion, heparin, in which an irreversible transformation to fibrils occurs and a large intra-Tau conformational change is observed in solution state preceding fibril formation.

RNA generally promotes complex coacervation whereas heparin effectively promotes fibrillization of Tau. The distinguishing effects between RNA (a polyphosphate) and heparin (a polysulfate) on Tau—coacervation versus fibrillization—may be an operational principle of Tau-polyanion association. Weak associations between multiples of Tau and RNA is consistent with the consensus property of a coacervate phase in which the hydration layer of the polyelectrolyte constituents remains intact, ensuring fluidity of the condensed phase, as well as reversibility between the dilute and condensed phase [14]. The Tau droplet state fits this biochemical portrait, so that Tau can reversibly and rapidly switch between the dilute solution and the dense droplet state, while involving minimal rearrangement of hydration water and protein conformations. The spontaneous complex coacervation from synthetic polyelectrolyte constituents can be entropy-driven according to several studies [6, 23, 28-30]. We found that Tau-RNA complex coacervation was enhanced at elevated temperatures, consistent with an entropy-driven reaction (data not shown). In fact, the observation of solution state-like protein conformational dynamics of Tau in the coacervate phase implies that the free energy penalty due to lowering of protein configurational entropy from protein ordering is minimal in the droplet state, and thus the cost for an entropy-driven complex coacervation reaction, paid by salt and/or water release, is small. Given this insight, we conclude that the transformation to insoluble aggregates from Tau droplets should be energetically more favorable than from dilute solution state, given the elevated protein concentration in the complex coacervate phase. Along these lines ten Wolde and Frenkel [31] have proposed that condensed liquid droplets serve as a "metastable crucible" to lower free energy barriers for crystal nucleation, while the discovery of the involvement of nucleic acids in coacervation-driven phase separation dates back to 1949 by Bungenberg de Jong [15]. Here, we identify a new state of Tau in which soluble Tau is reversibly stored in concentrated complex

coacervate droplets, readily bioavailable for cellular functions or vulnerable to pathological aggregation depending on the environmental cues at hand.

Materials and Methods

Cell culture

A total of eight samples were used for PAR-iCLIP studies. Four samples were human embryonic kidney (HEK 293T) cells that expressed either 4R2N (residues 1-441) wild type *tau* (one sample), 4R2N *tau* harboring the P301L mutation (one sample), and 4R1N *tau* harboring the P301L mutation fused to CFP (2 samples). Four samples were neurons derived from human induced pluripotent stem cells (hiPSCs) obtained by reprogramming dermal fibroblasts with virally transduced Yamanaka factors [32] that expressed wild type *tau*, two harboring a P301L *tau* mutation (with and without fused CFP) and one harboring the A152T variant [33, 34]. The hiPSC lines were karyotyped by Cell Line Genetics. Both wild type and P301L were normal males (46XY). A152T displayed a balanced three-way translocation of chromosomes 1, 13 and 7, which most likely occurred during the reprogramming process (46XY, t(1;13;7) (q31.2;q21;q36.3). Pluripotent cells were maintained in feeder-free conditions and cultured in BD Matrigel (BD Biosciences) coated six-well plates and fed with mTSER daily (Stemcell Technologies). Neuroectoderm differentiation utilized dorsomorphin and SB431542 (Sigma-Aldrich) for a week [35]. When neural-rosettes were clearly observable, the media was gradually replaced with neuronal induction media containing Knockout DMEM F12 with N2, and Glutamax 1X supplemented with laminin (Sigma-Aldrich) and maintained for an additional six days with every other day feeding. Neuro-rosettes were microdissected, and grown as neurospheres in the neuronal induction media supplemented with B27. Neurons were

differentiated from neurospheres by dissociating them into individual cells enzymatically with a 1/1 mixture of 0.25% trypsin / StemPro accutase (Thermo Fisher), and plated on Poly-L-Ornithin/Laminin coated six well plates at a density of 200,000 cells per well. Neuron differentiation and maturation were stimulated by the addition of 10 mM each of NT3, BDNF, and GDNF (Preprotech) to the neuronal growth media containing Neurobasal, N2 supplement, B27 Supplement and Glutamax. Neurons were fed twice per week by replacing half of the conditioned media with pre-warmed supplemented fresh media, and underwent maturation for at least five weeks. SH-SY5Y Neuroblastoma cells were plated as monolayers in DMEM/F12 medium with 10% FBS at 1x 10^6 per 10 cm dish, and the cells switched to neurobasal medium the next day and differentiated for seven days using 10 µM retinoic acid.

Antibodies

The Tau antibodies used were Tau-5 (1 mg/ml, Abcam); HJ 8.5 and HJ 9.2 (4.5 mg/ml and 2.8 mg/ml, both HJ antibodies are gifts from Dave Holtzman, Washington University); PHF-1 (gift from Peter Davis, Albert Einstein College of Medicine), MAP2 antibody (0.3 mg/ml, Proteintech™); CDK5 rabbit antibody (0.2 mg/ml, Santa Cruz); GFP rabbit antibody (5 mg/ml, Abcam); β-Actin (Sigma-Aldrich); mouse IgG_1 Alexa 680, (2 mg/ml, Invitrogen); mouse IgG Alexa 680 (2 mg/ml, Invitrogen); rabbit IgG 800 (1 mg/ml, Odyssey).

PAR-iCLIP

Cells were treated with 4-thiouridine (4SU) (Sigma-Aldrich) for 1h at a final concentration of 500 µM at 37°C, rinsed with ice-cold 1x PBS and irradiated one time with 400 mJ/cm^2 of 365 nm UV light on ice. 4-SU can enhance the cross-linking efficiency especially for proteins in

364 the cytoplasm [36-38]. The cells were centrifuged and the pellet stored at -80°C. The major steps
365 of PAR-iCLIP are listed in Fig. S6 and detailed in the supporting information. CLIP experiments
366 require an antibody, which can effectively immunoprecipitate Tau under stringent high salt wash
367 conditions. HJ 8.5 [39] raised against human Tau efficiently depleted Tau. With a dissociation
368 constant of 0.3 pM, HJ 8.5 pulled down Tau under the high-stringency purification conditions of
369 CLIP and remained bound to Tau throughout the procedure. Control experiments with GFP or
370 CDK5 antibody for the lysate expressing those proteins, or with HJ 8.5 antibody for lysates
371 without expressing Tau were always done in parallel to rule out false positive binding caused by
372 the beads. After immunoprecipitation, the cross-linked RNA was radiolabeled, the protein
373 separated on an SDS-PAGE gel, and transferred to nitrocellulose membrane and blotted. The
374 RNA-protein complexes from CLIP experiments (Fig. 1a-c) were cut from the blot, and the RNA
375 extracted followed by reverse transcription for library preparation [36]. The ^{32}P-labeled RNA
376 band was run on a polyacrylamide Tris-Borate Urea (TBU) denaturing gel to demonstrate the
377 confirm the size of the complex.
378
379 **Library preparation, deep sequencing and bioinformatics analysis of iCLIP**
380 The iCLIP libraries contained an experimental and a random barcode, which allowed
381 multiplexing and the removal of PCR duplicates. After the barcodes were introduced, sample and
382 control from one set of experiments were mixed to remove batch-to-batch variation. Libraries
383 were sequenced on an Ion Torrent Proton. Fastx collapser from FASTX-Toolkit was used to
384 collapse reads and filter replicates resulting from the PCR based on the random barcode. Reads
385 were separated into samples by the barcodes at the 5` ends of reads. The reverse transcription
386 primers sequences at both ends of the reads were trimmed with Cutadapt [40]. After trimming

the barcodes, reads with 18 bps or more were kept and counted as total unique reads, and aligned to the human genome (hg19) by Bowtie2 [41]. RseQC [42] was used to evaluate the quality of sequencing and mapping reads. Alignments with scores equal or greater than ten were kept for downstream analysis. Reads from these RNA pools were clustered by their alignments, and Pyicos tools [43] were used to identify the significant clusters. Clusters with at least five reads were retained and considered to contain target sites for RNA-Tau crosslinking. Gene models for RefSeq mRNAs, tRNAs, rRNAs were downloaded from the UCSC genome browser. miRNAs were downloaded from miRBase (release 20) and other categories of RNAs were download from Ensemble (release 73). Cross-link sites were identified as the termination site of the sequencing based on the iCLIP protocol [44]. Individual tRNA genes from the UCSC genome browser were predicted by using tRNAscan-SE v.1.23. The secondary structure for each tRNA was obtained from GtRNAdb (http://gtrnadb.ucsc.edu/).

Deep sequencing and analyses of small RNA expression in HEK cells and hiPSC-derived neurons

Small RNAs were extracted from HEK cells and hiPSC-derived neurons using miRNA isolation kit (mirVana^{TM}. Library preparation was adapted from the Ion RNA-seq v2 (Thermo Fisher) protocol. cDNAs with size range from 30-100 bp were selected and sequenced. Reads were aligned to both human genomes and tRNA sequences. When mapping reads to tRNA sequences, the Bowtie read aligner [45] protocol was used, in which a maximum of two mismatches were allowed. Reads aligned to tRNAs were counted and analyzed with a custom Perl scripts.

Recombinant Tau and Tau fragments

Full length recombinant human 4R2N Tau, N-terminal truncated, microtubule binding domain containing, K18 Tau (residues 244-372) and Δtau187 (residues 255-441 with a His-tag at the N-terminus) were used for *in vitro* studies. Methods for expression and purification of all recombinant Tau variants are detailed in the supplementary text. Two variants of Δtau187 were prepared via site-direct mutagenesis: Δtau187/322C contains a C291S mutation, leaving only one cysteine at site 322, and Δtau187G272C/S285C contains C291S, C322S, G272C and S285C mutations, leaving two cysteines at sites 272 and 285).

RNA gel mobility shift assay

The gel shift assay was performed with recombinant full length 4R2N Tau and chromatographically purified unacetylated yeast $tRNA^{Lys}$ (tRNA Probes) in 100 mM sodium acetate buffer at pH 7.0. The molar concentration of $tRNA^{Lys}$ was accurately re-measured with UV spectrophotometry after base-hydrolization to account for the hyperchromic effect from the secondary and tertiary structure of tRNA [20]. RNA43 was purchased in a kit (Pierce) with the sequence 5'-CCUGGUUUUUAAGGAGUGUCGCCAGAGUGCCGCGAAUGAAAAA-3' to represent a random sequence. The hydrolyzed tRNA and RNA43 samples were then quantified with UV spectrophotometry at 260 nm using an extinction coefficient of 0.025 $(\mu g/ml)^{-1}cm^{-1}$. For the gel shift assay, protein was incubated with tRNA at 37℃ for 10 minutes in the presence of 0.5 mM EDTA, 0.5 mM $MgCl_2$, 2 U SUPERase• In™ RNase Inhibitor (Thermo Fisher), 0.01% IGEPAL CA-630 (Sigma-Aldrich), and then applied to a TBE 8% Polyacrylamide Gel (Thermo Fisher). After gel separation, tRNA was stained with SYBR Gold II (Thermo Fisher). For quantitative analysis, the fraction of free and bound tRNA was quantified in ImageJ2 (National Institute of Health).

433

434 **Isothermal Titration Calorimetry (ITC) experiments**

435 Full length Tau or the K18 Tau were dialyzed overnight into a specified buffer for ITC (20 mM
436 ammonium acetate, pH 7). tRNA (from Baker's yeast, Sigma-Aldrich) was re-suspended in the
437 ITC buffer and concentration determined using a Nanodrop 1000 (Thermo Scientific).
438 Experiments were run on a Nano ITC (TA Instruments), in which 300 μM tRNA was titrated (5
439 μl injections) into a 1 ml protein solution of 30 μM Tau. Data was analyzed using the
440 NanoAnalyze v3.6 software (TA Instruments). After substracting the heat generated by tRNA
441 titration into empty buffer, the experimental data was fitted with an Independent binding model.
442 Experiments were repeated in triplicates and standard error of the mean reported.

443

444 **Spin labeling of Δtau187**

445 To achieve labeling with paramagnetic or diamagnetic probes, the protein was dissolved in 6 M
446 guanidinium hydrochloride and labeled overnight at 4°C using a 20-fold molar excess of the spin
447 label (1-oxyl-2,2,5,5-tetramethylpyrroline-3-methyl) methanethiosulfonate (MTSL, Toronto
448 Research Chemicals) or the diamagnetic analog of MTSL (1-Acetoxy-2,2,5,5-tetramethyl-δ-3-
449 pyrroline-3-methyl) methanethiosulfonate (Toronto Research Chemicals). Excess label was
450 removed using a PD-10 desalting column (GE Healthcare) equilibrated in a 20 mM ammonium
451 acetate buffer at pH 7.0. The protein was concentrated using a 3 kDa centrifugal filter (Amicon
452 UFC800396). The final protein concentration was determined by UV-Vis absorption at 274 nm
453 using an extinction coefficient of 2.8 $cm^{-1}mM^{-1}$, calculated from extinction coefficient of
454 Tyrosine [46]. The two variants Δtau187/322C and Δtau187G272C/S285C were spin labeled
455 with paramagnetic MTSL probes at the one or two cysteine sites, and are respectively referred to

as Δtau187/322C-SL and Δtau187G272C/S285C-SL_2. In order to achieve spin dilution, Δtau187/322C and Δtau187G272C/S285C were also labeled with the diamagnetic analogue of MTSL probes, and are referred to as Δtau187/322C/322C-DL and Δtau187G272C/S285C-DL_2. Images in Fig. 4a-b were taken using 400 μM Tau, 800 μg/ml poly(A) RNA and 30% glycerol in 20 mM ammonium acetate at pH 7.

Preparation of Tau-RNA complex coacervate

Droplets were formed in the 20 mM ammonium acetate buffer with NaCl concentration varying between 0 and 100 mM and glycerol concentration from 0 to 50% v/v. Solutions of Δtau187 or full length 4R2N Tau was mixed with tRNA (Baker's yeast, Sigma-Aldrich), poly(A) RNA or poly(U) RNA (Sigma-Aldrich) at varying protein, RNA, NaCl and glycerol concentrations in a 0.6 ml Eppendorf tube. RNAs were weighted out as powder and the mass concentration was calculated. The Tau:RNA mass ratio, the total concentration of Tau and RNA, as well as the NaCl salt concentration were optimized to maximize droplet formation, while choosing a total biopolymer density to avoid overlapping of droplets in the images to simplify the calculation of droplet coverage. Microscopy images were acquired at 10 minutes after mixing. A concentration of 19% v/v for the viscogen glycerol was determined to be an optimal concentration to ensure cryoprotection for DEER measurements carried out at ~80 K, while also ensuring maximal droplet formation at room temperature (Fig. S5b).

The charge of a peptide at a given pH was estimated by applying an algorithm adapted from Innovagen's Peptide Property Calculator (http://pepcalc.com/). All residues were assumed to have pKa values that are equivalent to the isolated residues (CRC Handbook of Chemistry and Physics, 87th ed). Charges of the C-terminus or N-terminus were estimated as -1 and +1,

479 respectively at both pH 6.0 and pH 7.0. The processing code is made available as supplementary
480 files on the free web (https://github.com/yanxianUCSB/PeptideChargeCalculator).
481
482 **Bright-field microscopy of Tau-RNA droplets**
483 Immediately after mixing Tau in a 0.6 ml Eppendorf tube with RNA under droplet forming
484 conditions (established above) and ensuring thorough mixing, 1 μl of this mixture was applied to
485 a microscope slide that is closed with a cover slide gapped by two layers of double-side sticky
486 tape to generate a liquid sample region with consistent thickness. The microscope slide was kept
487 at room temperature for 10 minutes with the cover slide facing down, during which the particles
488 within the liquid sample region settled down onto the surface of the cover slide. Images were
489 taken with a 12-bit CCD camera across the entire sample liquid region near the surface of the
490 cover slide using an inverted compound microscope (Olympus IX70). Before imaging, Köhler
491 illumination was applied and the focus close to the surface of the cover slide optimized to
492 enhance the contrast between the dark droplets and the bright background.
493
494 **Confocal microscopy of Tau-RNA droplets**
495 For confocal microscopy, Δtau187/322C was fluorescently labeled (Δtau187/322C-FL) with
496 Alexa Fluor 488 C_5 Maleimide (Thermo Fisher) at the same 322 site as Δtau187/322C-SL. 50
497 μM of Δtau187/322C-FL was mixed with 350 μM Δtau187/322C-SL at a 1:7 molar ratio in order
498 to prevent saturation. 800 μg/ml of poly(A) RNA was further added to this Tau solution,
499 resulting in droplet formation in the 20 mM ammonium acetate buffer and in the presence of 20
500 mM NaCl. 10 μL of the mixture was pipetted and put on a microscope slide with a cover slide

gapped by double-sided sticky tape. Confocal images were acquired using a spectral confocal microscope (Olympus Fluoview 1000).

Droplet quantification from image analysis

To quantify the amount of droplet formed under the given experimental condition of interest, images were taken by a 12-bit CCD camera of an inverted compound microscope (Olympus IX70), and recorded in TIF format. With illumination and focus optimized, droplets settling on the cover slide have lower intensity than their surrounding on the images. An image of the 20 mM ammonium acetate buffer was taken to calculate the average intensity to set as threshold in order to classify different parts of the image into droplets and buffer. For each image, the area of the droplets was divided by the total area of the image, generating a % droplet coverage value on the cover slide. Droplets with eccentricity above 0.9 or equivalent diameter below 1 μm were filtered out in order to reduce false reading. The MATLAB code is made available as supplementary files on the free web (https://github.com/yanxianUCSB/DropletAnalysis).

Continuous wave (cw) Electron Paramagnetic Resonance (EPR)

Cw EPR relies on the anisotropy of nitroxide radical's Larmor frequency and hyperfine coupling that makes its lineshape highly sensitive to the local dynamics, orientation and confinement of a nitroxide-based spin label tethered to the protein. Cw EPR measurements were carried out with Δtau187/322C-SL using a X-band spectrometer operating at 9.8 GHz (EMX, Bruker Biospin) and a dielectric cavity (ER 4123D, Bruker Biospin). Samples were prepared by either mixing 200 μM Δtau187/322C-SL with 300 μM unlabeled Δtau187/322C (to generate 40% spin labeled sample) or by using 500 μM Δtau187/322C-SL (100% labeled). Viscogen was added to the

sample to achieve either 19% v/v glycerol (for the droplet samples) or 30% v/v sucrose (for the aggregated samples) matching the DEER conditions. Tau samples under droplet forming condition were prepared by adding 1.5 mg/ml RNA, and Tau samples under aggregation-inducing conditions prepared by adding 125 μM heparin (11 kDa average MW, Sigma-Aldrich). A sample of 3.5 μL volume was loaded into a quartz capillary (VitroCom, CV6084) and sealed at one end with critoseal and the other with beeswax, and then placed in the dielectric cavity for measurements. Cw EPR spectra were acquired using 2 mW of microwave power, 0.3 gauss modulation amplitude, 150 gauss sweep width and 25 scans for signal averaging.

Double Electron Electron Resonance (DEER)

DEER measurements were performed on a Q-band pulsed EPR spectrometer operating at 32 GHz (E580, Bruker Biospin) equipped with a QT2 resonator (measurements done by courtesy of Bruker Biospin). Samples were prepared by mixing 50 μM Δtau187G272C/S285C-SL_2 with 500 μM analog-labeled Δtau187G272C/S285C-DL_2 at a 1:10 molar ratio to achieve spin-dilution and avoid artifacts from unwanted inter-protein spin distances. For DEER, Tau samples under droplet forming condition were prepared by adding 1.65 mg/ml RNA and ensuring 19% v/v glycerol concentration, and Tau samples under aggregation-inducing conditions prepared by adding 137.5 μM heparin and ensuring 30% v/v sucrose concentration. 40 μL samples containing 550 μM concentration of Tau were loaded into a quartz capillary (2.4 mm od x 2 mm id) and flash frozen in liquid nitrogen after 20 minutes of incubation at room temperature. DEER measurements were conducted using the dead-time free four-pulse DEER sequence at 80 K, using 22 ns (π/2) and 44 ns (π) observe pulses and a 30 ns (π) pump pulse. The raw DEER data was processed using Gaussian fitting via DeerAnalysis2013 [47].

Quantification of fibril using Thioflavin T assay

18 μM Δtau187 was mixed with 100 μg/ml poly(U) RNA and incubated at room temperature at presence of 4 μM Thioflavin T for over 3 days with or without additional 100 mM NaCl. Fluorescence at 485 nm was measured via Infinite 200 Pro plate reader (Tecan).

Transfer RNA transfection

Neuronal cultures were transfected with 20U of bovine liver tRNA (Sigma-Aldrich) per six well plate using lipofectamine 2000 transfection reagent (Thermo Fisher) following the manufacturer's protocol. Control cells were transfected in equal conditions in the absence of nucleic acid (Mock transfection). Mock transfected cells were lysed as described below, with or without 20U tRNA added to the lysis buffer.

Sarkosyl insolube Tau isolation and western blotting

Separation of sarkosyl insoluble Tau was done as described in the literature [48, 49]. Briefly, adherent neuronal cell cultures were lysed with an ice-cold high salt/high sucrose Tris HCl buffer (0.8 M NaCl, 10% Sucrose, 10 mM Tris HCl pH 7.4) containing a 1X Protease Inhibitor Cocktail, and a 1X Phosphatase Inhibitor Cocktail. Lysis proceeded at 4°C for 30 min before detachment with a cell scraper, followed by mechanical dissociation using a micropipette. Immediately afterwards, the lysates were centrifuged at 4°C 3000 x g for 15 min in a microcentrifuge. The clear supernatants were collected and sampled (Input). Sodium lauroyl sarcosinate (Sigma-Aldrich) was then added to the supernatants to a final concentration of 1%, followed by a brief vortexing. Samples were incubated at 4°C with continuous rocking. Samples were then

centrifuged at 4°C for 2 h at 170000 x g in a Beckman Coulter 70.1 Ti rotor. Sarkosyl soluble supernatants (Sol.) were collected. Sarkosyl insoluble (Ins.) pellets were resuspended in 2X sample loading buffer (250 mM Tris HCl pH 6.8, 10% Glycerol, 10% SDS, 0.5% bromophenol blue, 20 mM DTT) and heated to 95°C for 10 min. The previously collected input and the sarkosyl soluble fractions were diluted with the same sample loading buffer, and heated under similar conditions. Proteins were separated on a 10% SDS-PAGE, transferred to Nitrocellulose membranes, and blotted with either PHF-1 or β–actin antibody.

Data availability

The data that support the findings of this study are available from the corresponding authors on request.

Acknowledgments

We are grateful to the Tau consortium for financial support to K.S.K. and S.H., D. M. Holtzman, Washington University School of Medicine for the generous gift of HJ 8.5 antibody and P. Davies, Albert Einstein College of Medicine for PHF-1 antibody. This work was supported by the 2011 NIH Director New Innovator Award to S.H and made use of the Material Research Laboratory (MRL) Central Facilities supported by the National Science Foundation (NSF) through the Materials Research Science and Engineering Center under Grant DMR 1121053. We acknowledge the use of the NRI-MCDB Microscopy Facility and the Spectral Laser Scanning Confocal supported by the Office the Director, National Institutes of Health (NIH) under Award # S10OD010610. The authors declare no competing financial interests.

593

Figure 1

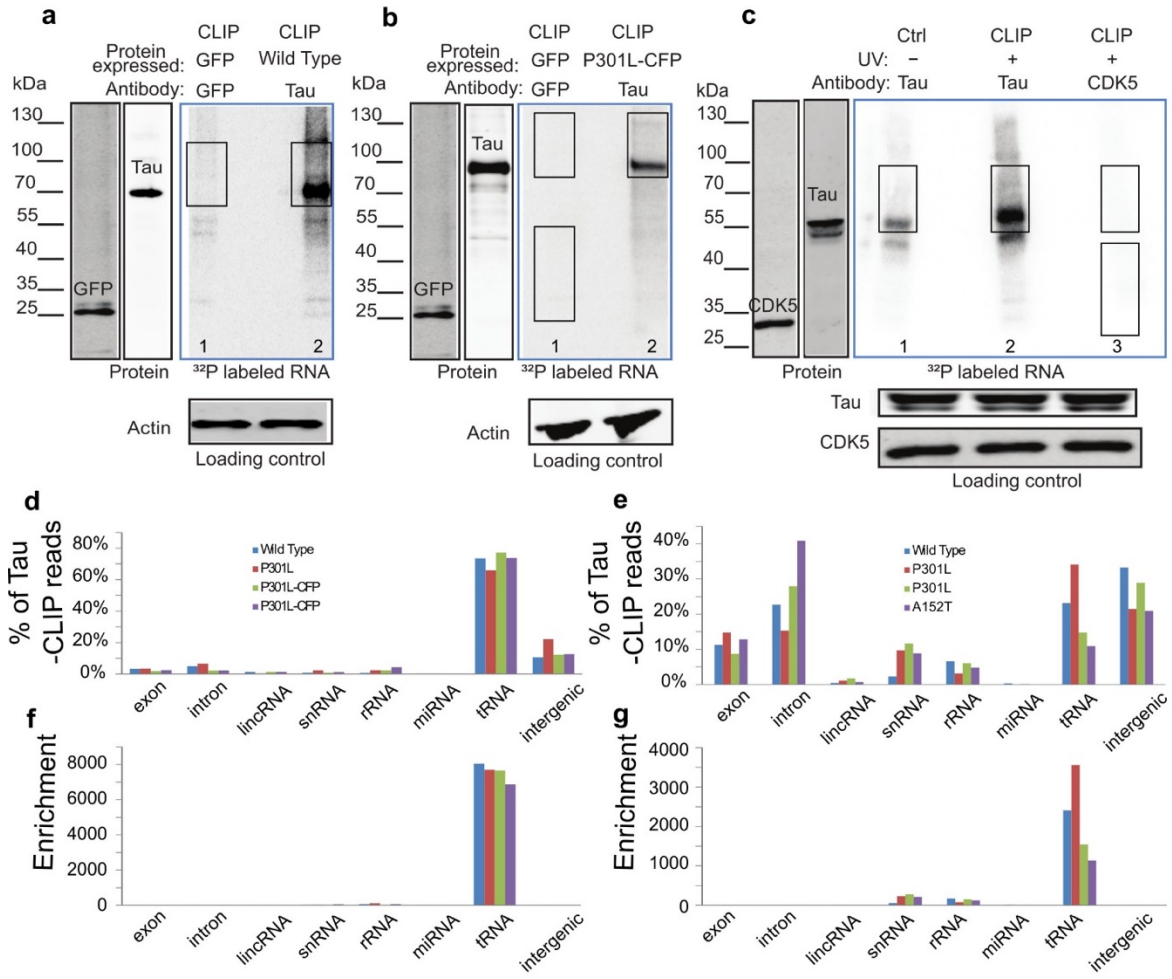

594

595 **Fig. 1: Tau PAR-iCLIP in Tau expressing HEK cells and hiPSC-derived neurons.** Phosphor
596 images in the blue frame display crosslinked ^{32}P-labelled RNA in the nitrocellulose blot. (a-c)
597 PAR-iCLIP with wild type Tau (a) or Tau P301L-CFP (b) and endogenous wild type Tau in
598 hiPSC-derived neurons (c) (lane 2 in a-c), PAR-iCLIP for GFP (lane 1 in a-b), CDK5 (lane 3 in c)
599 and no UV control (lane 1 in c). The antibodies anti-Tau HJ 8.5, anti-GFP and anti-CDK5 were
600 used for protein precipitation. No RNase was added. A small RNA signal was visible in the
601 absence of cross-linking in hiPSC-derived neurons (lane 1, c), suggesting a small portion of

602 RNA may associate with Tau *in vitro* after cell lysis. The RNA-protein complexes from CLIP
603 marked by a rectangle was cut from the blot for DNA library preparation. (d-e) % of Tau-CLIP
604 reads that mapped to eight human genome regions in HEK cells (d) and hiPSC-derived neurons
605 (e). (f-g) Enrichment of tRNA in Tau-CLIP of HEK cells (f) and hiPSC-derived neurons (g) as
606 discussed in text.
607

607

Figure 2

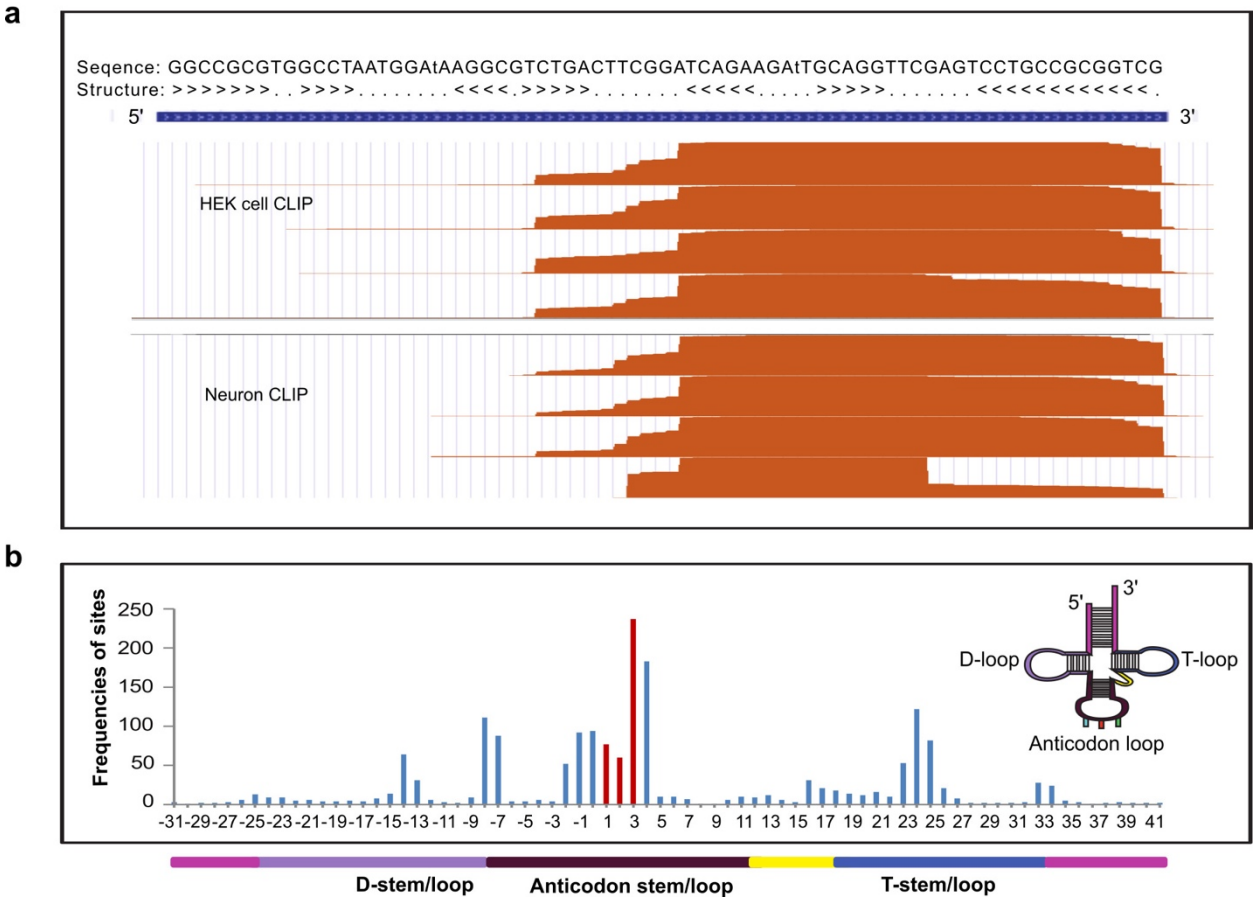

608

609

610 **Fig. 2: Enrichment of tRNA in PAR-iCLIP data.** (a) CLIP cDNA reads for tRNA

611 chr15.tRNA4-ArgTCG are found in all CLIP samples and demonstrate a similar pattern of

612 crosslinking. (b) Analysis of crosslinked sites along tRNA secondary structure demonstrates the

613 anticodon preference, anticodon (colored red) designated as position 1-3 for alignment purpose.

614 The colored illustration of tRNA secondary structure is displayed as inset and below the x-axis in

615 1-D dimension.

616

Figure 3

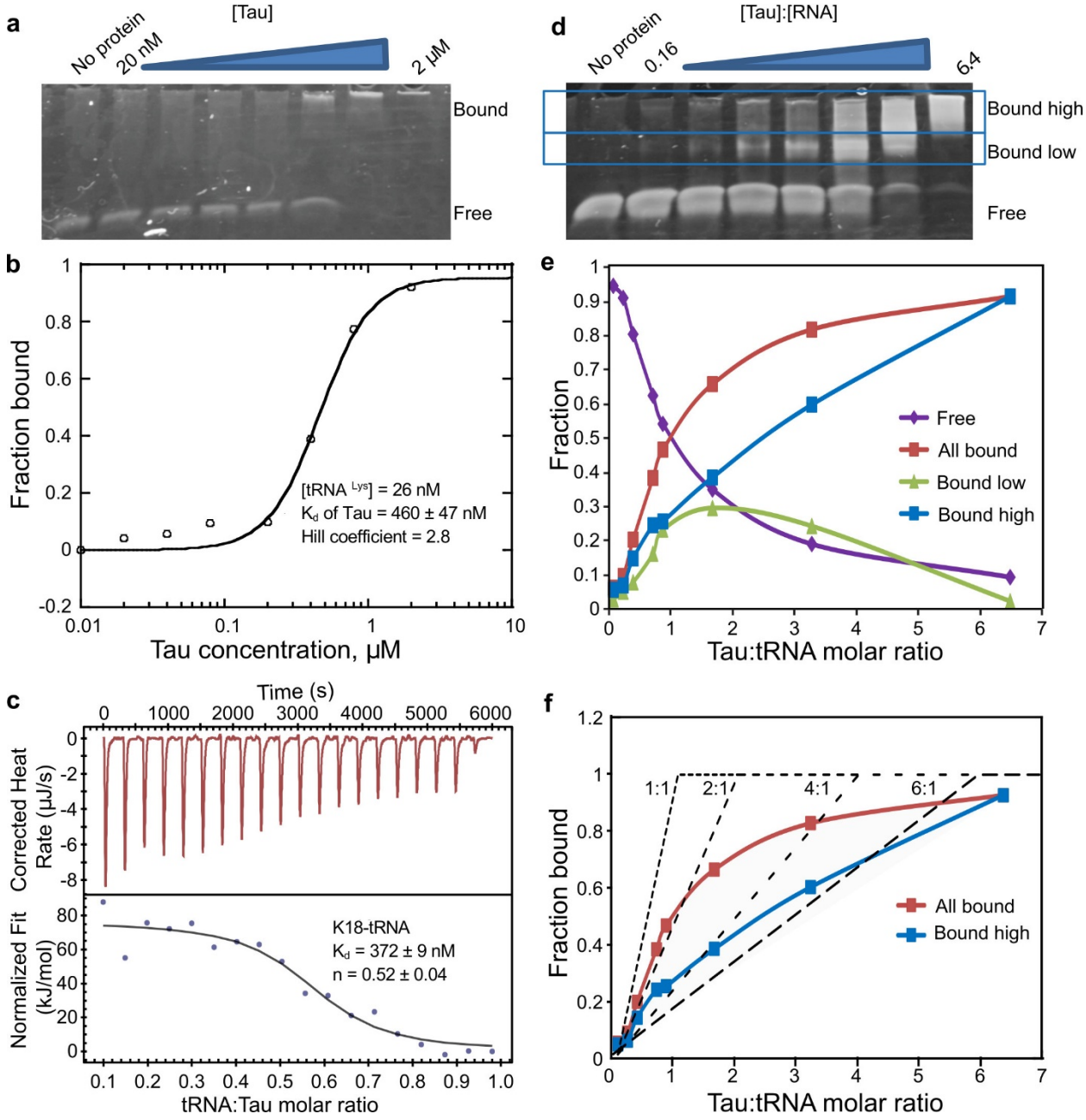

Fig. 3: Tau tRNA binding by gel shift assay and ITC. (a) Direct titration experiment shows full length protein Tau induces a mobility shift in $tRNA^{Lys}$. (b) The fraction of bound tRNA plotted as a function of the monomeric Tau concentration and fit to the Hill equation, y = 1/ [1+

623 $(K_d / x)^n$. (c) Yeast tRNA was titrated into solutions of K18 Tau in an ITC experiment. The top
624 panels show the raw incremental-titration. The area under each peak is integrated and plotted
625 against the molar tRNA:Tau ratio and fitted to an independent binding model (the bottom panel).
626 (b-c) Standard error of the mean (SEM) is reported, n=3. (d) Stoichiometry shift assay varying
627 full length protein Tau:RNA molar ratio while tRNA in 2.6 μM. (e) Fraction of bound tRNA in d
628 is plotted over the molar Tau:tRNA ratio. (f) Fraction of bound Tau plotted as a function of
629 Tau:tRNA molar ratios and compared to the theoretical saturation binding curves (dotted
630 lines) with 1:1 to 6:1 protein:RNA molar stoichiometry.

Figure 4

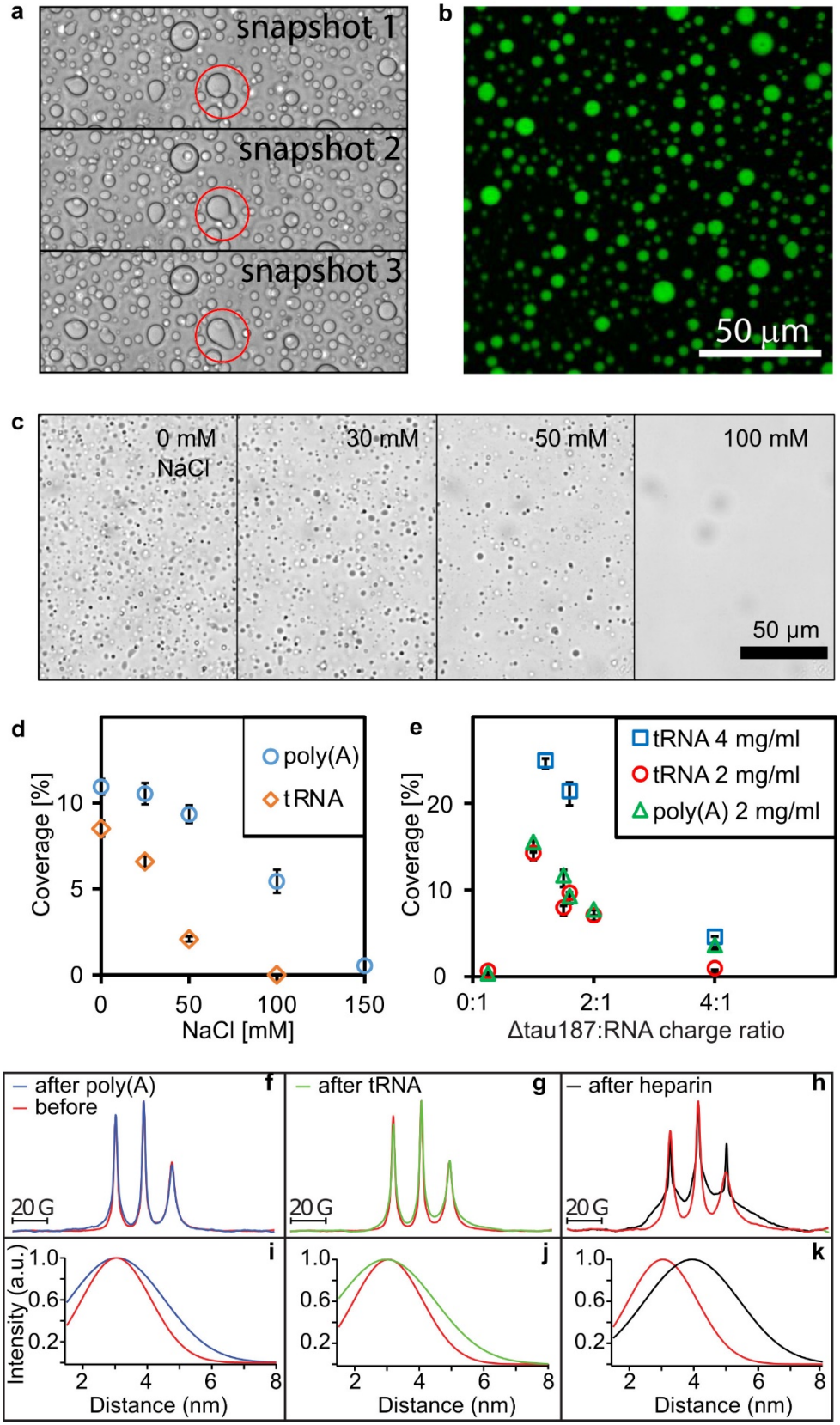

Fig. 4: Tau and RNA forms droplet *in vitro*. (a) Bright field snapshots of droplets from Δtau187 and poly(A) showing two droplets seamlessly fusing (highlighted with red circle). (b) Confocal microscopy image of Δtau187 labeled with Alexa-488 in the droplets as in (a). c) Representative bright-field images of Tau-RNA droplet with varying [NaCl]. d) Droplet coverage with poly(A) or tRNA with varying [NaCl] and e) varying Δtau187: RNA charge ratios. Δtau187:RNA in c-d were maintained at a charge ratio of 1.2:1 and a total mass concentration of 2 mg/ml. Error bars in (d) and (e) represent the standard deviation from n=3. (f-k) CW EPR spectra obtained at room temperature of Δtau187 in droplets formed with 1.5 mg/ml poly(A) RNA (f) and 1.5 mg/ml tRNA (g) is unaltered from solution before adding RNA. CW EPR line shape upon adding 125 μM heparin (h) show dramatic line broadening. DEER of Δtau187-SL_2 in droplets formed with 1.5 mg/ml poly(A) RNA (i) and 1.5 mg/ml tRNA (j), as well as upon incubation with 137.5 μM heparin (k).

644

Figure 5

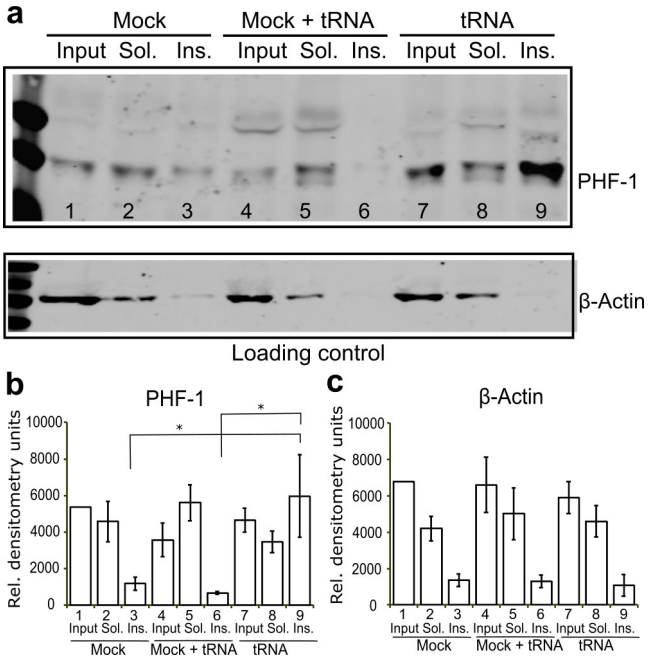

645

646 **Fig. 5: tRNA transfection accumulates sarkosyl insoluble Tau in hiPSC derived neurons.** (a)
647 Cells transfected with tRNA but not cells transfected in the absence of nucleic acids (Mock, lane
648 3) present an evident accumulation of sarkosyl insoluble Tau (tRNA, lane 9). Addition of tRNA
649 to the lysis buffer is insufficient to increase the Tau present in the insoluble fractions (Mock +
650 tRNA, lane 6). (b-c) Quantification of PHF-1 Tau (b) and β-actin (c) level are shown. Error bar
651 represents standard error of the mean. * $p < 0.05$, n=5.

652

References

1. Goedert M, Jakes R, Spillantini MG, Hasegawa M, Smith MJ, Crowther RA. Assembly of microtubule-associated protein tau into Alzheimer-like filaments induced by sulphated glycosaminoglycans. Nature. 1996;383(6600):550-3.
2. Kampers T, Friedhoff P, Biernat J, Mandelkow EM, Mandelkow E. RNA stimulates aggregation of microtubule-associated protein tau into Alzheimer-like paired helical filaments. FEBS Letters. 1996;399(3):344-9. doi: http://dx.doi.org/10.1016/S0014-5793(96)01386-5.
3. Wang X, Wang D, Zhao J, Qu M, Zhou X, He H, et al. The Proline-Rich Domain and the Microtubule Binding Domain of Protein Tau acting as RNA Binding Domains. Protein & Peptide Letters. 2006;13:679-85.
4. Sanders David W, Kaufman Sarah K, DeVos Sarah L, Sharma Apurwa M, Mirbaha H, Li A, et al. Distinct Tau Prion Strains Propagate in Cells and Mice and Define Different Tauopathies. Neuron. 2014;82(6):1271-88. doi: http://dx.doi.org/10.1016/j.neuron.2014.04.047.
5. Goedert M. Alzheimer's and Parkinson's diseases: The prion concept in relation to assembled Aβ, tau, and α-synuclein. Science. 2015;349(6248):1255555. doi: 10.1126/science.1255555. PubMed PMID: 26250687.
6. Patel A, Lee Hyun O, Jawerth L, Maharana S, Jahnel M, Hein Marco Y, et al. A Liquid-to-Solid Phase Transition of the ALS Protein FUS Accelerated by Disease Mutation. Cell. 2015;162(5):1066-77. doi: 10.1016/j.cell.2015.07.047.
7. Kato M, Han TW, Xie S, Shi K, Du X, Wu LC, et al. Cell-free formation of RNA granules: Low complexity sequence domains form dynamic fibers within hydrogels. Cell. 2012;149(4):753-67. doi: 10.1016/j.cell.2012.04.017.
8. Lee K-H, Zhang P, Kim Hong J, Mitrea DM, Sarkar M, Freibaum BD, et al. C9orf72 Dipeptide Repeats Impair the Assembly, Dynamics, and Function of Membrane-Less Organelles. Cell. 2016;167(3):774-88.e17. doi: http://dx.doi.org/10.1016/j.cell.2016.10.002.
9. Lin Y, Mori E, Kato M, Xiang S, Wu L, Kwon I, et al. Toxic PR Poly-Dipeptides Encoded by the C9orf72 Repeat Expansion Target LC Domain Polymers. Cell. 2016;167(3):789-802.e12. doi: http://dx.doi.org/10.1016/j.cell.2016.10.003.
10. Molliex A, Temirov J, Lee J, Coughlin M, Kanagaraj Anderson P, Kim Hong J, et al. Phase Separation by Low Complexity Domains Promotes Stress Granule Assembly and Drives Pathological Fibrillization. Cell. 2015;163(1):123-33. doi: http://dx.doi.org/10.1016/j.cell.2015.09.015.
11. Kim HJ, Kim NC, Wang YD, Scarborough EA, Moore J, Diaz Z, et al. Mutations in prion-like domains in hnRNPA2B1 and hnRNPA1 cause multisystem proteinopathy and ALS. Nature. 2013;495(7442):467-73. doi: 10.1038/nature11922.
12. Pak Chi W, Kosno M, Holehouse Alex S, Padrick Shae B, Mittal A, Ali R, et al. Sequence Determinants of Intracellular Phase Separation by Complex Coacervation of a Disordered Protein. Molecular Cell. 2016;63(1):72-85. doi: http://dx.doi.org/10.1016/j.molcel.2016.05.042.
13. Jho Y, Yoo HY, Lin Y, Han S, Hwang DS. Molecular and structural basis of low interfacial energy of complex coacervates in water. Advances in Colloid and Interface Science. 2016. doi: http://dx.doi.org/10.1016/j.cis.2016.07.003.

14. Huang K-Y, Yoo HY, Jho Y, Han S, Hwang DS. Bicontinuous Fluid Structure with Low Cohesive Energy: Molecular Basis for Exceptionally Low Interfacial Tension of Complex Coacervate Fluids. ACS Nano. 2016;10(5):5051-62. doi: 10.1021/acsnano.5b07787.
15. Bungenberg de Jong HG. Colloid Science. In: Kruyt HR, editor. II. Amsterdam: Elsevier Publishing Co. Inc; 1949. p. 335-432.
16. Hwang DS, Zeng H, Srivastava A, Krogstad DV, Tirrell M, Israelachvili JN, et al. Viscosity and interfacial properties in a mussel-inspired adhesive coacervate. Soft Matter. 2010;6(14):3232-6. doi: 10.1039/C002632H.
17. Overbeek JT, Voorn MJ. Phase separation in polyelectrolyte solutions; theory of complex coacervation. J Cell Physiol Suppl. 1957;49(Suppl 1):7-22; discussion, -6. PubMed PMID: 13449108.
18. Dehmelt L, Halpain S. The MAP2/Tau family of microtubule-associated proteins. Genome Biol. 2005;6(1):204.
19. Friedersdorf M, Keene J. Advancing the functional utility of PAR-CLIP by quantifying background binding to mRNAs and lncRNAs. Genome Biology. 2014;15(1):R2.
20. Ryder SP, Recht MI, Williamson JR. Quantitative analysis of protein-RNA interactions by gel mobility shift. Methods in molecular biology (Clifton, NJ). 2008;488:99-115. doi: 10.1007/978-1-60327-475-3_7. PubMed PMID: PMC2928675.
21. Zucconi BE, Ballin JD, Brewer BY, Ross CR, Huang J, Toth EA, et al. Alternatively Expressed Domains of AU-rich Element RNA-binding Protein 1 (AUF1) Regulate RNA-binding Affinity, RNA-induced Protein Oligomerization, and the Local Conformation of Bound RNA Ligands. Journal of Biological Chemistry. 2010;285(50):39127-39.
22. Okunola HL, Krainer AR. Cooperative-Binding and Splicing-Repressive Properties of hnRNP A1. Molecular and Cellular Biology. 2009;29(20):5620-31.
23. Aumiller WM, Pir-Cakmak F, Davis BW, Keating CD. RNA-based coacervates as a model for membraneless organelles: Formation, properties, and interfacial liposome assembly. Langmuir. 2016. doi: 10.1021/acs.langmuir.6b02499.
24. Ortony JH, Hwang DS, Franck JM, Waite JH, Han S. Asymmetric Collapse in Biomimetic Complex Coacervates Revealed by Local Polymer and Water Dynamics. Biomacromolecules. 2013;14(5):1395-402. doi: 10.1021/bm4000579.
25. Pérez M, Valpuesta JM, Medina M, Montejo de Garcini E, Avila J. Polymerization of τ into Filaments in the Presence of Heparin: The Minimal Sequence Required for τ - τ Interaction. Journal of Neurochemistry. 1996;67(3):1183-90. doi: 10.1046/j.1471-4159.1996.67031183.x.
26. von Bergen M, Barghorn S, Biernat J, Mandelkow E-M, Mandelkow E. Tau aggregation is driven by a transition from random coil to beta sheet structure. Biochimica et Biophysica Acta (BBA) - Molecular Basis of Disease. 2005;1739(2–3):158-66. doi: http://dx.doi.org/10.1016/j.bbadis.2004.09.010.
27. Qin J, Priftis D, Farina R, Perry SL, Leon L, Whitmer J, et al. Interfacial Tension of Polyelectrolyte Complex Coacervate Phases. ACS Macro Letters. 2014;3(6):565-8. doi: 10.1021/mz500190w.
28. Priftis D, Megley K, Laugel N, Tirrell M. Complex coacervation of poly(ethylene-imine)/polypeptide aqueous solutions: Thermodynamic and rheological characterization. Journal of Colloid and Interface Science. 2013;398:39-50. doi: http://dx.doi.org/10.1016/j.jcis.2013.01.055.

29. Aberkane L, Jasniewski J, Gaiani C, Scher J, Sanchez C. Thermodynamic Characterization of Acacia Gum−β-Lactoglobulin Complex Coacervation. Langmuir. 2010;26(15):12523-33. doi: 10.1021/la100705d.
30. Xu AY, Melton LD, Jameson GB, Williams MAK, McGillivray DJ. Structural mechanism of complex assemblies: characterisation of beta-lactoglobulin and pectin interactions. Soft Matter. 2015;11(34):6790-9. doi: 10.1039/C5SM01378J.
31. Wolde PRt, Frenkel D. Enhancement of Protein Crystal Nucleation by Critical Density Fluctuations. Science. 1997;277(5334):1975.
32. Takahashi K, Yamanaka S. Induction of Pluripotent Stem Cells from Mouse Embryonic and Adult Fibroblast Cultures by Defined Factors. Cell. 126(4):663-76. doi: 10.1016/j.cell.2006.07.024.
33. Coppola G, Chinnathambi S, Lee JJ, Dombroski BA, Baker MC, Soto-Ortolaza AI, et al. Evidence for a role of the rare p.A152T variant in MAPT in increasing the risk for FTD-spectrum and Alzheimer's diseases. Human Molecular Genetics. 2012;21(15):3500-12.
34. Fong H, Wang C, Knoferle J, Walker D, Balestra Maureen E, Tong Leslie M, et al. Genetic Correction of Tauopathy Phenotypes in Neurons Derived from Human Induced Pluripotent Stem Cells. Stem Cell Reports. 2013;1(3):226-34. doi: 10.1016/j.stemcr.2013.08.001. PubMed PMID: PMC3849235.
35. Mak SK, Huang YA, Iranmanesh S, Vangipuram M, Sundararajan R, Nguyen L, et al. Small molecules greatly improve conversion of human-induced pluripotent stem cells to the neuronal lineage. Stem Cells Int. 2012;2012:140427. doi: 10.1155/2012/140427. PubMed PMID: 22567022; PubMed Central PMCID: PMCPMC3339118.
36. Huppertz I, Attig J, D'Ambrogio A, Easton LE, Sibley CR, Sugimoto Y, et al. iCLIP: Protein–RNA interactions at nucleotide resolution. Methods. 2014;65(3):274-87. doi: http://dx.doi.org/10.1016/j.ymeth.2013.10.011.
37. Tollervey JR, Curk T, Rogelj B, Briese M, Cereda M, Kayikci M, et al. Characterizing the RNA targets and position-dependent splicing regulation by TDP-43. Nat Neurosci. 2011;14(4):452-8. doi: http://www.nature.com/neuro/journal/v14/n4/abs/nn.2778.html#supplementary-information.
38. Hafner M, Landthaler M, Burger L, Khorshid M, Hausser J, Berninger P, et al. Transcriptome-wide identification of RNA-binding protein and microRNA target sites by PAR-CLIP. Cell. 2010;141(1):129-41. doi: 10.1016/j.cell.2010.03.009. PubMed PMID: 20371350; PubMed Central PMCID: PMC2861495.
39. Yanamandra K, Kfoury N, Jiang H, Mahan TE, Ma S, Maloney SE, et al. Anti-tau antibodies that block tau aggregate seeding in vitro markedly decrease pathology and improve cognition in vivo. Neuron. 2013;80(2):402-14. doi: 10.1016/j.neuron.2013.07.046. PubMed PMID: PMC3924573.
40. Martin M. Cutadapt removes adapter sequences from high-throughput sequencing reads. EMBnet journal. 2011;17(1):10-2.
41. Langmead B, Salzberg SL. Fast gapped-read alignment with Bowtie 2. Nat Meth. 2012;9(4):357-9. doi: 10.1038/nmeth.1923 http://www.nature.com/nmeth/journal/v9/n4/abs/nmeth.1923.html#supplementary-information.
42. Wang L, Wang S, Li W. RSeQC: quality control of RNA-seq experiments. Bioinformatics. 2012;28(16):2184-5. doi: 10.1093/bioinformatics/bts356.

783 43. Althammer S, González-Vallinas J, Ballaré C, Beato M, Eyras E. Pyicos: a versatile
784 toolkit for the analysis of high-throughput sequencing data. Bioinformatics. 2011;27(24):3333-
785 40.
786 44. Konig J, Zarnack K, Rot G, Curk T, Kayikci M, Zupan B, et al. iCLIP reveals the
787 function of hnRNP particles in splicing at individual nucleotide resolution. Nat Struct Mol Biol.
788 2010;17(7):909-15. doi:
789 http://www.nature.com/nsmb/journal/v17/n7/abs/nsmb.1838.html#supplementary-information.
790 45. Langmead B, Trapnell C, Pop M, Salzberg S. Ultrafast and memory-efficient alignment
791 of short DNA sequences to the human genome. Genome Biology. 2009;10(3):R25.
792 46. Fasman GD, editor. Handbook of Biochemistry and Molecular Biology. 3rd ed.
793 Cleveland, OH.: CRC Press; 1976.
794 47. Jeschke G, Chechik V, Ionita P, Godt A, Zimmermann H, Banham J, et al.
795 DeerAnalysis2006—a comprehensive software package for analyzing pulsed ELDOR data.
796 Applied Magnetic Resonance. 2006;30(3):473-98. doi: 10.1007/BF03166213.
797 48. DeTure M, Ko L-w, Easson C, Yen S-H. tau Assembly in Inducible Transfectants
798 Expressing Wild-Type or FTDP-17 tau. The American Journal of Pathology. 2002;161(5):1711-
799 22. PubMed PMID: PMC1850799.
800 49. Carrettiero DC, Hernandez I, Neveu P, Papagiannakopoulos T, Kosik KS. The Co-
801 chaperone BAG2 Sweeps PHF Insoluble Tau from the Microtubule. Journal of Neuroscience.
802 2009;29(7):2151-61. doi: 10.1523/JNEUROSCI.4660-08.2009. PubMed PMID: PMC2768429.

803